RSC Publishing Faraday Discussions

Donor-Acceptor Preassociation, Excited State Solvation Threshold, and Optical Energy Cost as Challenges in Chemical Applications of Photobases

Journal:	*Faraday Discussions*
Manuscript ID	FD-ART-11-2018-000215.R1
Article Type:	Paper
Date Submitted by the Author:	06-Dec-2018
Complete List of Authors:	Hunt, Jonathan; University of Southern California, Chemistry Tseng, Cindy; University of Southern California, Chemistry Dawlaty, Jahan; University of Southern California, Chemistry

Journal Name

ARTICLE TYPE

Cite this: DOI: 10.1039/xxxxxxxxxx

Donor-Acceptor Preassociation, Excited State Solvation Threshold, and Optical Energy Cost as Challenges in Chemical Applications of Photobases

Jonathan Ryan Hunt,[a] Cindy Tseng,[a] and Jahan M Dawlaty*[a]

Received Date
Accepted Date

DOI: 10.1039/xxxxxxxxxx

www.rsc.org/journalname

Photobases are molecules with increased pK_a in the excited state that can serve to transduce light energy into proton removal capability. They can be used to control chemical reactions using light, such as removing protons from a catalytic site in reactions that are rate-limited by proton transfer. We identify and explore several major challenges toward their practical applications. Two important challenges are the need for pre-association (or ground state hydrogen bonding) between the proton donor and the photobase, and the need for excited state solvation of the photogenerated products. We investigate these two challenges with the photobase 5-methoxyquinoline as the proton acceptor and a low-pK_a alcohol, 2,2,2-trifluroethanol, as the proton donor. We vary the concentration of the donor in a background non-hydrogen-bonding solvent. Using absorption spectroscopy, we have identified that the donor-acceptor concentration ratio must exceed 100:1 to achieve appreciable ground state hydrogen bonding. Interestingly, emission spectroscopy reveals that the onset of ground state hydrogen bonding does not guarantee successful excited state proton transfer. It takes an additional order of magnitude increase in donor-acceptor ratio to achieve that goal, revealing that it is necessary to have excess donor molecules to reach the solvation threshold for the photogenerated products. The next challenge is reducing the large ground-excited state energy gap, which often requires UV photons to drive proton transfer. We show experimental and computational data comparing the photobasicity and optical energy gap for a few N-aromatic heterocyclic photobases. In general, we find that reducing the energy gap by increasing the conjugation size necessarily reduces photobasicity, while adding substituents of varying electron-withdrawing strengths allows some fine-tuning of this effect. The combination of these two factors provide a preliminary design space for creating new photobasic molecules.

Proton transfer is important in a wide range of chemical and biological phenomena. Often redox reactions, especially those that are relevant for energy storage, are coupled with proton transfer and cannot be explained as electron transfer in isolation. Proton gradients are the driving force for a range of processes in living organisms, most notably synthesis of ATP. Most proposals on storing light energy in chemical bonds require driving multi-electron and multi-proton reactions. Given the importance of proton transfer in such diverse areas, understanding optical control over proton transfer is not only of fundamental importance, but it also opens opportunities for applications. Understanding excited state proton transfer in photoacids and photobases is a fundamental first step towards these goals.

Photoacids, which are molecules that become acidic in the electronically excited state, have been well-known for several decades[1–6]. Prime examples are conjugated systems such as pyrenols[7–9] and naphthols[10–12], in which the OH functionality becomes more acidic in the excited state, often by more than 6 pK_a units. Photoacids have been used in a wide range of applications. Some examples are triggering acid initiated protein folding[13,14], acid-catalyzed reactions[15], pH-dependent enzymatic reactions[16,17], synthetic organic reactions[18,19], generation of a protonic potential difference with light[20], and photo-control of protonic conductivity of electrolytes with light[21].

Photobases are molecules that achieve the reverse effect and become more basic in the excited state. Some examples are quinolines[22–27], Schiff bases[28], acridines[29–32], 3-styrylpyridine[33], xanthone[34], and curcumin[35]. Both fundamental studies and applications of photobases to chemical problems

[a] University of Southern California, 920 Bloom Walk, Los Angeles, US. Tel: 213-740-9337 ; E-mail: dawlaty@usc.edu

† Electronic Supplementary Information (ESI) available: [details of any supplementary information available should be included here]. See DOI: 10.1039/b000000x/

are far limited compared to their photoacid counterparts. They offer rich prospects for applications, for example in catalytic reactions that are rate-limited by sluggish proton removal and require use of strong bases. One may use photobases to create the proton removal drive using light in the vicinity of such catalysts. In a recent work, we have installed pendant photobases on an Ir-core organometallic catalyst with this goal in mind[36]. In another work, we have used photobases to deprotonate a family of alcohols, with the broader goal of generating reactive alkoxides using light[37].

Despite promises, several challenges exist in the way of applying photobases as optically driven proton removal agents in catalysis or for inducing large scale pH change. We note four of these challenges. The first challenge is pre-association of the proton donor and photobase. Due to the often limited excited state lifetime of the photobase, it is desirable for it to be pre-hydrogen bonded with the target proton donor in the ground state. Upon optical excitation, the proton is then removed and the photobase is not required to search for and find its target during its limited excited state lifetime.

The second challenge is solvation of the photogenerated products or dissociation of ion-pairs after successful proton transfer. In order for the initial proton transfer step to occur, certain solvation conditions must be met. Often for downstream chemistry to proceed on a deprotonated target molecule, that molecule must then dissociate from the conjugate acid form of the photobase. Such dissociation must beat the excited state lifetime of the photobase. It is possible to tune this dissociation by the choice of the medium that would allow faster diffusion and better screening of the Coulomb attraction between ion pairs. Previously, in a work on photoinduced proton conductivity using photoacids we have shown that the separation of ions within the excited state lifetime is possible[38]. Such considerations are needed when photobases are required to induce bulk pH changes.

The third challenge is the energetic cost of proton removal. Many photobases operate with photon energies higher than 3 eV (<400 nm). While for certain applications using such high energies may not pose a problem, it is desirable to lower this energetic cost. This necessitates finding out how excited state pK_a scales with optical gap in various families of photobases.

The fourth challenge is the limited excited state lifetime of photobases, and is intimately tied to the challenges described above. A photobase, after successful deprotonation of a target molecule, will only retain the proton for as long as it remains in the excited state, which could be several nanoseconds for singlet states. Upon return to the ground state, it releases the proton back. To give the often sluggish chemical steps a chance to proceed in the aftermath of a proton transfer, it is desirable to hold on to the removed proton for longer. An immediate strategy is to extend the excited state lifetime by intersystem crossing and creating triplets. However, the pK_a of triplet states are often lower than that of singlets, and one must find strategies to optimize the balance between pK_a* and excited state lifetime.

In this work, we will take steps towards understanding the first three of the above challenges - the pre-association of photobase and proton donors, the solvation threshold for photogenerated products, and the energetic cost of optical excitation. We will present experimental and theoretical results for better understanding these problems and propose strategies to mitigate them.

In section I, we will review the thermodynamics and kinetics of photobasicity in quinolines. In section II we will show our experimental work that quantifies pre-association and threshold for excited state proton transfer. We will briefly discuss proposed strategies to overcome the limitations posed by these problems. In section III we will discuss that while increasing the conjugation size of the chromophore may decrease the optical gap, it will also reduce the thermodynamic drive for proton removal. We will propose strategies for finding a balance between these opposing effects.

1 Brief Overview of Thermodynamics and Kinetics of Photobases

To set the stage for the rest of this work, in this section we review the fundamental ideas of excited state proton transfer, with emphasis on photobasicity.

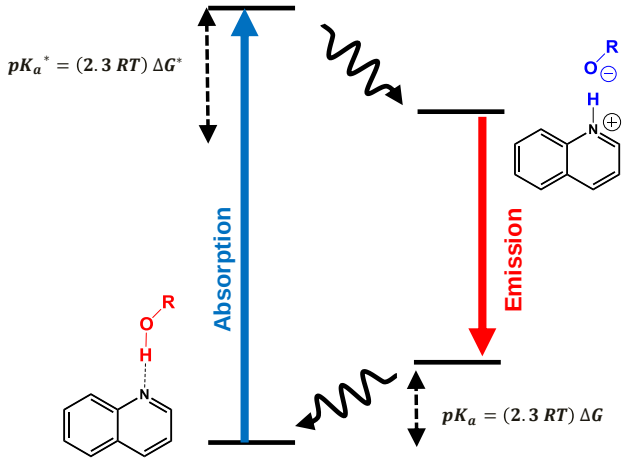

Fig. 1 The Forster thermodynamic cycle for proton transfer in a quinoline photobase. The excited state pK_a* can be inferred from energy gaps of protonated and unprotonated forms and the ground state pK_a.

The excited state acidity and basicity is commonly inferred from a thermodynamic cycle originally reported by Förster[39], depicted in figure 1. The approximations and conditions for the validity of the Forster cycle are discussed in several references[2,40]. In brief, the Forster cycle for a photobase starts with unprotonated form that absorbs light, undergoes proton transfer with a forward thermodynamic drive ΔG^*, emits from the protonated form, and finally releases the proton and returns to the initial state. The energy difference ΔG between protonated and unprotonated forms is determined by measuring the pK_a of the molecule by conventional ground state titration and using $pK_a = \Delta G/(2.3RT)$. Absorption and emission spectroscopy is used to determine the energy gaps between ground and excited states of protonated and unpro-

tonated forms. These numbers allow for estimating the gap ΔG^*, which is related to the excited state pK_a by $pK_a^* = \Delta G^*/(2.3RT)$. As a convenient reference number, an energy gap of 477 cm^{-1} (59 meV or nearly 10 nm in the visible range) corresponds to one unit of pK_a at $T = 298$ K. Various approximation exist that help with determination of 0-0 vibronic gaps for the unprotonated and protonated forms in the presence of broad absorption and emission spectra. Often a large separation of time-scales exist between proton transfer times (few tens of picoseconds) to relaxation to ground state times (few nanoseconds). This justifies the conventional use of equilibrium thermodynamic language of pK_a^* for expressing the drive for proton transfer in the excited state.

Even though the Forster cycle described above is quite useful, it only informs us about the existence of a thermodynamic drive for proton transfer. In fact, the energy gap for the protonated form in the cycle need not be determined by an emission spectrum, and instead can be determined by measuring the absorption gap of a molecule that is protonated in the ground state by lowering the pH. Therefore, a Forster cycle can be constructed even if excited state proton transfer does not occur due to kinetic limitations.

Several processes can compete against proton transfer in the excited state. It seems reasonable to think a free energy relation (FER) must exist between the speed of protonation and the thermodynamic drive or pK_a* of the molecule. However, experiments suggest that the excited state dynamics is often more complicated due to a variety of competing factors. In our previous work, we have followed two strategies to investigate kinetic trends for proton transfer in the quinoline family. First, we have tuned the pK_a* of a quinoline photobase family by varying the electron withdrawing strength of a substituent (as describe by its Hammett parameter) attached to the conjugated rings[26]. According to the Forster analysis for this series, the quinoline pK_a* linearly decreased with increasing Hammett parameter. However, there was no clear trend in the kinetics of proton transfer, and in some members signatures of proton transfer were convoluted with triplet dynamics in the excited state[27]. Second, we have varied the pK_a of the proton donor by choosing a series of alcohols, while keeping the photobase molecule the same[37]. In this case, a clearer trend in kinetics was observed, with the more acidic donors undergoing faster proton transfer. Apart from the intramolecular factors, solvation of the conjugate base and conjugate acid likely influences the kinetics. In brief, Forster analysis is an important and powerful tool for assessing the thermodynamic drive of photobases. However, it is unable to predict the competing kinetic pathways, and barriers to proton transfer.

2 Pre-Association in the Ground State and Solvation Threshold for Excited State Proton Transfer

Successful proton transfer in the excited state often requires the proton donor and acceptor to be hydrogen bonded or pre-associated in the ground state. Achieving such ground state pre-association is often difficult, especially when the proton donor exists in small concentrations in a background solvent. Pre-association is necessary due to the typically short (several ns) lifetimes of singlet excited states of the photobase. The excited states of photobases likely have larger drives for complexation than their ground states. However, if the diffusion time necessary to find a target proton donor partner is longer than the excited state lifetime, the photobase will return to the ground state without successful deprotonation.

To understand the problem of pre-association, we consider a proton donor and a photobase in a background non-hydrogen-bonding solvent. Although the enthalpy of hydrogen bonding favors complexation of the photobase with the donor, the Gibbs energy of solvation of the two partners likely works against it. Even if the enthalpy of solvation of separated species compared to the solvation of the complex is negligible, the entropy of the dissociated species is vastly larger compared to the complex. Therefore, the entropic drive for decomplexation can overwhelm the enthalpic drive for hydrogen bonding. To enforce a significant population of hydrogen bonded complexes against this entropic drive, one may increase the concentration of the donor.

We have two purposes in this section. First, we will demonstrate the threshold concentration ratio between proton donor and photobase that is necessary to create a significant ground state hydrogen bonded population countering the entropy of dissociation. Second, we will demonstrate that slightly above this threshold concentration of the donor, even though ground state hydrogen bonded complexes are formed, excited state deprotonation still fails. We will show that to achieve successful excited state deprotonation, the concentration of donor must go even higher. The excess donors are necessary to solvate the conjugate base of the proton donor after proton transfer. We will demonstrate the threshold concentration of donors that makes this solvation possible.

Our photobase in this study is 5-methoxyquinoline (MeOQ). It has a pK_a* of approximately 15.5 and has been studied previously by us[26,27,37]. The proton donor is 2,2,2-trifluoroethanol (TFE), which is a low pK_a alcohol (pK_a=12.4) that is known in the literature as a good hydrogen-bond donor[41]. We have shown in a previous work that MeOQ deprotonates TFE rather rapidly ($\sim$ 2 ps) due to the large thermodynamic drive for deprotonation ($pK_a^* - pK_a = 3.1$). The background non-hydrogen-bonding solvent is dichloromethane (DCM). The concentration of the photobase MeOQ is kept at 5×10^{-5} M, which is a convenient value for absorption and emission measurements. The concentration of the donor TFE relative to the photobase MeOQ is scanned over several orders of magnitude (1:1 to 200000:1 with respect to MeOQ) in the background DCM solvent. For each solution of given concentration ratio, absorption spectra were measured for signs of ground state hydrogen bonding, while emission spectra were monitored for identifying the threshold of excited state deprotonation.

We studied the growth of the ground state hydrogen-bonded complex using absorption spectroscopy as shown in Figure 2. As the ratio of donor TFE to photobase MeOQ increases, the spectrum of the photobase red-shifts, indicating hydrogen bond formation with TFE. Most of the shift is seen before TFE constitutes a significant portion of the total solvent volume, showing that this shift is not due to average modification of the dielectric constant.

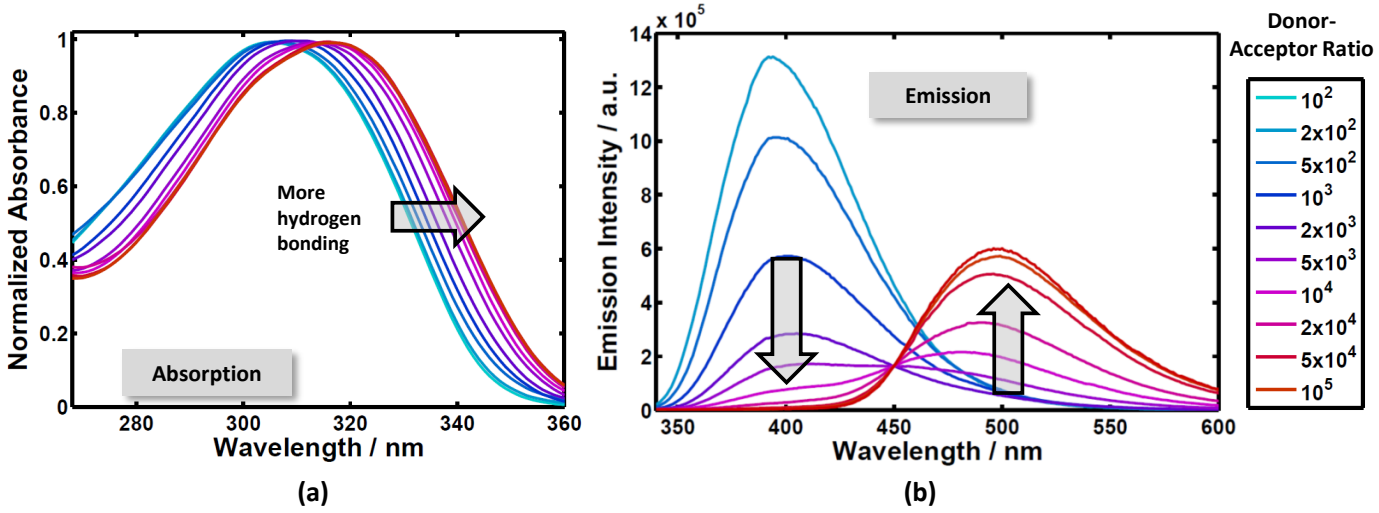

Fig. 2 (a) Absorption spectra of the photobase MeOQ as a function of TFE concentration. Hydrogen bonded photobase has a red-shifted spectrum. Therefore, with increasing ratio of proton donor TFE the spectrum red-shifts. (b) Emission spectra of the photobase MeOQ. Protonated photobase in the excited state has a distinctly red shifted emission, which increases with increasing donor TFE concentration.

Furthermore, since TFE and DCM have roughly the same dielectric constant[42,43] (8.55 and 8.93, respectively), we can be certain that the large shifts seen in these experiments (> 10nm) are due to hydrogen-bonding.

As discussed in the experimental methods section, this continuous red shift of the absorption spectrum can be used to identify the relative populations of the hydrogen-bonded and non-hydrogen-bonded photobases. The blue trace in figure 3 shows the fraction of the hydrogen bonded photobases as a function of increasing TFE concentration.

The figure shows that hydrogen bonding does not begin until there are approximately 200 TFE molecules for every photobase MeOQ molecule. It takes a TFE to photobase ratio of 2000:1 for approximately half of the photobase molecules to hydrogen bond, and it takes a ratio of 50,000:1 to see hydrogen bonding reach the same level as in bulk TFE. These observations indicate that, even though there is an enthalpic drive for pre-association by hydrogen bonding, dissociation is far more favored and a great excess of hydrogen bond donor is necessary to overcome the dissociation entropy. Since pre-association is necessary for excited state proton transfer, this difficulty in making hydrogen bonded complexes has an impact on the application of photobases for driving deprotonation reactions where the donor is dilute. Such problems are likely to be even greater for weaker hydrogen-bond donors, compared to the strong hydrogen bond donor in our work.

To identify the threshold concentration for proton transfer, we have measured emission spectra as a function of relative ratio of donor to photobase (figure 2.b). Fortunately, the protonated and unprotonated forms of the photobase have distinctly different emission spectra, with the protonated form red shifted by approximately 100 nm, which makes analysis of the relative populations of the protonated and unprotonated forms relatively convenient as described in the methods section. Since in the ground state there is no proton transfer, emission from protonated (unprotonated) form indicates the degree of successful (unsuccessful) proton transfer in the excited state. We were particularly interested in whether emission from protonated MeOQ would track the ground state hydrogen bonding pattern. In other words, we aim to answer whether excited state proton transfer is possible for all ground state hydrogen-bonded complexes, even those at the onset of the hydrogen bonding threshold.

The red trace in figure 3, shows the rise of the protonated MeOQ emission as a function of TFE concentration. It is clearly seen that there is a distinct lag between the onset of ground state hydrogen bonding and successful excited state proton transfer. To achieve successful deprotonation in the excited state, the concentration of the donor must be much higher than that required to achieve ground state hydrogen bonding.

At the onset of H-bonding, noticeable small red-shifts and decrease in the intensity of the emission spectrum of MeOQ were observed. However, no rise in the emission of the protonated form of MeOQ were seen. We therefore assign these early spectral changes exclusively to hydrogen bond formation. Although hydrogen-bonding was first observed in the absorption spectra at a ratio of 200:1, emission from the protonated form of MeOQ was not observed until a ratio of 5,000:1, a ratio where approximately 75% of the MeOQ molecules were hydrogen bonded in the ground state. The lag seen between hydrogen-bond complex formation threshold and proton transfer threshold is more than an order of magnitude in TFE concentration.

This lag between ground state hydrogen bond formation and successful excited state proton transfer points towards the importance of solvation of the photogenerated products (conjugate base of the donor and conjugate acid of the acceptor) after proton transfer. If only a single donor is present in a background non-hydrogen-bonding solvent, solvation of the conjugate base is difficult. However, if a small cluster of several donor molecules exists in the vicinity of the donor-acceptor complex, it becomes much easier to solvate the resulting conjugate base due to the formation of a small hydrogen bond network. This scenario is shown

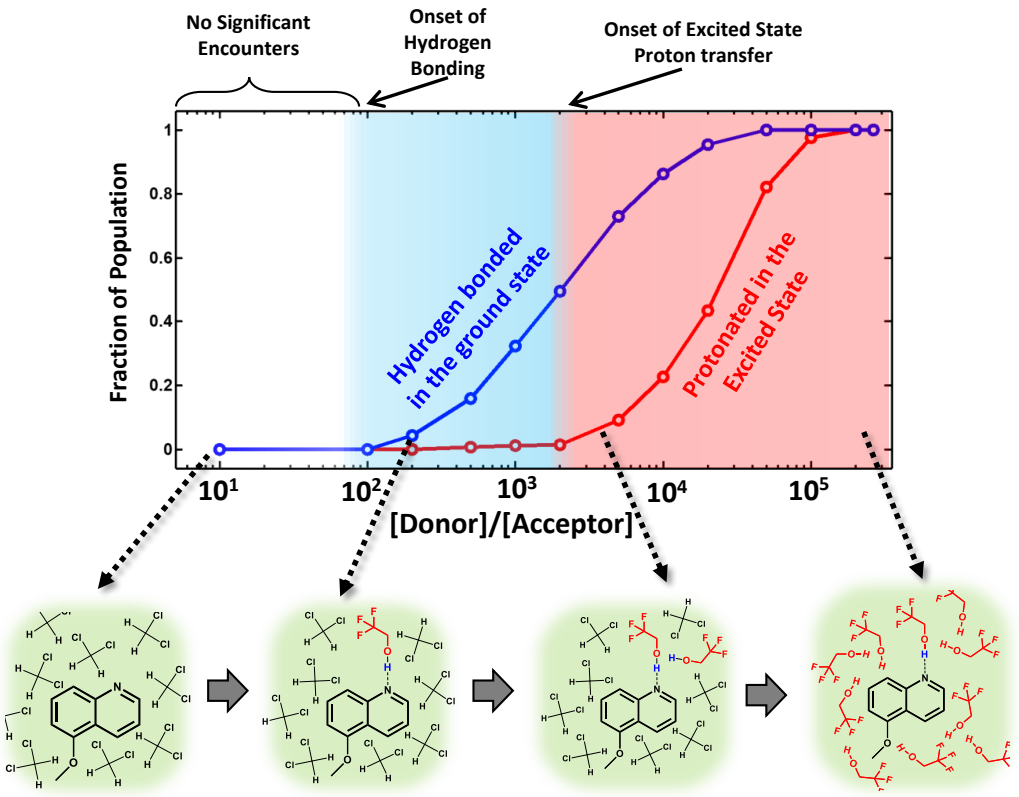

Fig. 3 Data highlighting the importance of pre-association in the ground state and the solvation threshold for successful excited state deprotonation. The blue line is extracted from the red shift of the hydrogen bonded absorption spectra and indicates the rise of the relative fraction of ground state hydrogen bonded complexes. The red line is extracted from the rise of the emission of the protonated form and indicates the fraction of excited state molecules that can successfully deprotonate the donor. To begin hydrogen bonding in the ground state, a large excess of nearly 100:1 of proton donor to photobase is needed. A lag of nearly one order of magnitude between the onset of hydrogen bonding and the onset of emission from protonated form indicates that more than one molecule of donor in the solvation shell of a donor-acceptor complex are needed to solvate the resulting conjugate base and therefore allowing successful deprotonation. The cartoon in the bottom indicates progression of increasing the donor concentration.

in figure 4. The ability of small alcohol clusters to solvate charges has been reported in the photoacid literature previously[44].

Emission from the protonated form of MeOQ begins while there is still a appreciable population of non-hydrogen bonded MeOQ in the ground state and while the contribution of TFE to the solution volume is still small (approximately 1%). Therefore, any alcohol clusters that form near MeOQ are likely to be small as well, especially since the enthalpic drive for cluster formation is likely smaller than the enthalpic drive for hydrogen bonding with the photobase. Previous literature has studied the kinetics of photoacid dissociation as a function of alcohol concentration and determined that two alcohol molecules are capable of solvating the resulting protonic charge[44]. Therefore, it is reasonable and logical to estimate that two TFE molecules participate in the clusters required to solvate the excited state photobasic products studied here. A pictoral representation of the proposed two-molecule TFE cluster can be seen in figure 4.

We reiterate that the dielectric constants of the background solvent and TFE are very close to each other[42,43] (8.55 and 8.93 respectively). It is therefore unlikely that the solvation threshold can be attributed to the interpolated dielectric constant between the two solvents. We also point out that hydrogen bonding to the methoxy terminal of our photobase is possible. The contribution of that hydrogen bond to stabilizing the protonated excited state of the photobase is likely minimal and, if non-negligible, is probably slightly unfavorable due to the resulting dislocation of electron density away from the aromatic rings and therefore away from the photobasic nitrogen atom.

These results reveal the challenge of pre-association and solvation of photogenerated products in practical applictions of photobases. Even if there is a large thermodynamic drive for deprotonation of a proton donor (as there is in this scenario), dissociation entropy must be overcome with a large excess of the donor before the necessary pre-association is achieved. Furthermore, solvation of the photogenerated products must be ensured for excited state proton transfer.

Based on the above, two strategies are proposed for overcoming these problems. The first is directly tethering the photobase to a location where it is needed, thereby avoiding the necessity for pre-association. For example, a photobase can be covalently bound to the ligand periphery of an organometallic catalyst as a pendant moiety. The center of action for deprotonation is the

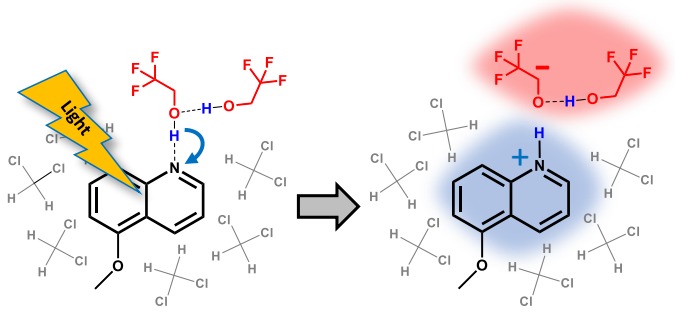

Fig. 4 The data supports a model in which at least two proton donors form a hydrogen bond complex with a photobase. Upon optical excitation and proton capture from one of the donors, the resulting anion is stabilized by a second donor. A photobase hydrogen bonded with only a single donor is unable to achieve this. For that reason, proton transfer becomes possible at a higher threshold concentration of donors than the threshold to create singly hydrogen bonded complexes.

catalytic metal. When a substrate binds to the metal and the reaction progresses to the stage that it becomes limited by proton transfer, excitation of the photobase can facilitate proton removal from the substrate. Recently, work by us and our collaborators has resulted in the synthesis of a model iridium complex with a pendant photobase[36]. Even though the catalytic properties of the created complex is still unclear, it was shown that the pendant quinoline maintains its photobasicity in the vicinity of the metal center. This is a first step toward rationally incorporating photobases in catalytic centers. The second strategy is the use of non-hydrogen bonding solvents with high dielectric constants, since they will not compete for hydrogen bonding with the donor and will assist with charge separation and screening of the photogenerated conjugate acid and base. In addition to these restrictions, optical transparency of the solvent also needs to be accounted for to ensure that light reaches the photobase.

3 Energy Cost for Photodriven Deprotonation

The second challenge in using photobases in applications is the energy cost of the optical excitation. Typical unprotonated quinoline photobases have their first absorption in the range of 290 nm - 350 nm (3.5-4.2 eV). In some applications using such high energy photons may be justified, particularly when alternate photochemical processes do not interfere. However, it is desirable to reduce the necessary excitation energy. In this section we address this problem using two approaches. The first is reducing the ground-excited state energy gap by increasing the size of the N-heterocyclic conjugated systems. The second approach is addition of substituents to the aromatic system. We will show that while both of these handles can tune the excitation energy, they also have a large effect on photobasicity. The combination of these two factors provide a preliminary design space for creating new photobasic molecules.

To begin with, we demonstrate a correlation between experimental $\Delta pK_a = pK_a^* - pK_a$ and computed electron density build up on nitrogen upon photoexcitation $\Delta q_N = q_N^* - q_N$. As shown in figure 5 through visualization of electron density differences, there is an increase in electron density on the heteroatomic nitrogen of N-heterocycles upon excitation to the L_b state. In figure 6, we show the experimentally measured ΔpK_a values determined from Forster cycle analysis for various 5-substituted quinolines plotted versus the computationally calculated change in electron density Δq_N of the L_b state upon excitation, determined using Lowdin analysis. The L_b state was chosen because it is known to be the photobasic state in N-heterocyclic photobase molecules, as discussed in a previous work[26]. A clear linear relation is observed between the excess charge build up on nitrogen and the ΔpK_a. This correlation is mechanistically justified since the excess negative charge on nitrogen in the excited state can be reasonably interpreted as the initial drive for attracting the proton. We also include the experimentally measured Forster cycle ΔpK_a for acridine and its corresponding computed Δq_N in the plot. Even though it is an entirely different molecule with a larger conjugation size, it roughly falls within the trend for the substituted quinoline family. This correlation shows that excess charge density Δq_N can reasonably be used as a computational proxy for photobasicity when exploring the wide space of N-heterocyclic aromatic photobases.

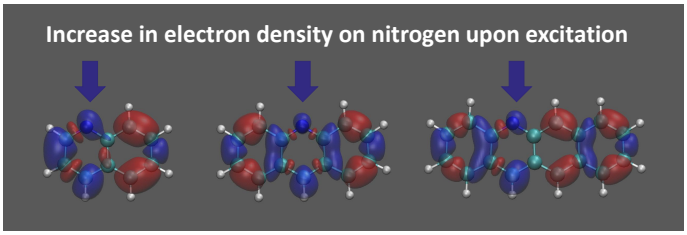

Fig. 5 Electron density difference maps of three N-heterocycles (quinoline, acridine, benzacridine) for the L_b excited electronic state. Blue surfaces indicate an increase in electron density and red surfaces indicate a decrease in electron density. For all molecules, an increase in the electron density of the heteroatom is observed.

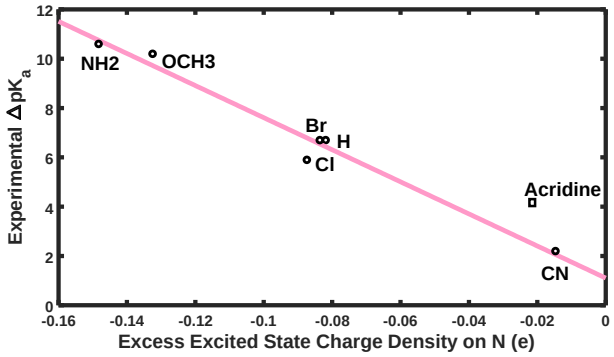

Fig. 6 Experimental ΔpK_a of substituted quinolines determined from Forster cycle analysis, versus their calculated excess charge density build up on nitrogen upon photoexcitation Δq_N using Lowdin analysis. The experimental ΔpK_a and computed Δq_N for acridine is also included, which, even though is a different conjugation size, falls reasonably near the trend line.

Armed with the above knowledge, we proceed to use Δq_N

as a convenient computational proxy for ΔpK_a to explore the conjugation size and substituents parameter space of N-heterocyclic aromatics. We have chosen quinolines, acridines, and $\alpha-$napthoquinoline (benzacridine), which have two, three, and four conjugated rings, respectively (figure 7). We performed calculations on these molecules with a range of substituents of varying electron-withdrawing strengths. The substituent locations on the conjugated systems were chosen as shown in figure 7. We chose the 5 position for the quinoline substituents because of the existence of both experimental Forster analysis and ultrafast kinetic data for proton transfer for the 5-R-quinoline family reported by us previously[37,45]. The positions on acridine and benzacridine are the analogous positions with respect to the heteroatom. The substituents chosen in the order of increasing electron withdrawing power (Hammett parameter) are $-NH_2, -OCH_3, -Cl, -Br, -CN$. Unsubstituted molecules (Hammett parameter of zero) are also included.

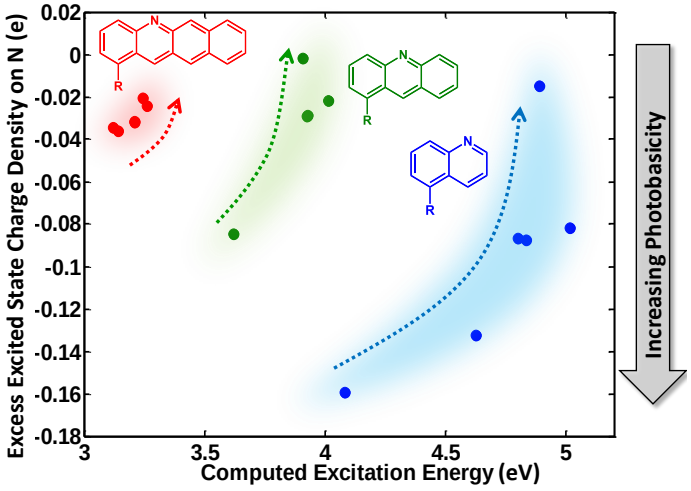

Fig. 7 The influence of conjugation size and substitution on photobasicity, serving as a guide for designing photobasic N-heterocyclic molecules. Excess electronic charge build up on nitrogen upon photoexcitation is plotted versus the electronic energy gap. The excess negative charge correlates well with the experimental Forster cycle ΔpK_a values (figure 6) and therefore can serve as a proxy for photobasicity. As the size of the conjugated system is increased, the excitation energy goes down as expected. However, the excess electron density on nitrogen and correspondingly photobasicity decreases. The dotted arrows for each molecule indicate the direction of increasing electron withdrawing power of the substituent R. Generally, more electron withdrawing substituents polarize the electron density away from nitrogen and result in lower photobascity. The larger the conjugated system, the less sensitive its nitrogen is to varying substituents. Finally, we note that the computed energies are systematically overestimated by nearly 0.7 eV compared to experimental values. Here the relative trends, rather than the absolute values, are meaningful.

Several important lessons may be learned from figure 7. First, as expected, the excitation energy gap is reduced as we move to larger conjugated systems. However, this reduction in excitation energy correlates with a reduction of the excess electron density on nitrogen Δq_N upon excitation, which can be interpreted as a smaller ΔpK_a. This observation is logically justifiable, because in a large N-heterocyclic system a single electronic excitation is spread over a larger space and the share of electron density moved to nitrogen from that excitation is smaller. The lesson here is that the size of the conjugated system is intimately coupled with photobasicity and cannot be independently tuned.

The next observation in the figure is the influence of substituents on energy gap and photobasicity. First, it can be clearly observed that the substituents make a larger difference for the smaller conjugated systems. For the 4-ring system ($\alpha-$napthoquinoline), the substituents barely change the excitation gap and the excess charge on nitrogen, while for quinoline a much wider spread in both of these quantities is observed. This is justifiable since for the larger systems, the substituent is a smaller perturbation to both the ground and excited states of the molecule. The lesson from this observation is that while one may use the substituent effect to tune photobasicity and electronic energy gap, the tunability range is wider for smaller systems.

Next, we note that as the electron-withdrawing strength (Hammett parameter) of the substituent is increased (the direction of the dotted arrows in figure 7), the photoexcited excess charge on nitrogen $\Delta q_N = q_N^* - q_N$ is diminished. It is expected that increasing the Hammett parameter should reduce both q_N and q_N^*. The figure shows that their differences is also reduced with increasing Hammett parameter. This can only be true if q_N^* is more sensitive to Hammett parameter and reduces more rapidly compared to q_N. This is justifiable because the excited states of molecules are more polarizable and therefore more sensitive to electron withdrawing effects of the substituents. The lower Hammett values (i.e. electron releasing groups) make the nitrogen more basic in the ground state. The figure shows that such groups also have larger photobasicity. The lesson learned from this observation is that within the N-heterocyclic aromatic family, stronger bases are in general also stronger photobases.

Finally, while figure 7 is useful as a design guide, a cautionary points must be made about its interpretation. The first point is that the diagram is only constructed for optically active singlet states, which also happen to be mostly the lowest lying excited states in these molecules. The photoexcited molecules may be capable of intersystem crossing and going to triplet states. We have previously explored the importance of triplet states in the excited state kinetics of substituted quinolines[27]. Acridines are also known to undergo singlet to triplet transitions[46]. When transition to triplet states is faster than proton transfer, proton transfer is out-competed by intersystem crossing even if the proton transfer is thermodynamically favorable. It is possible for a triplet state to be photobasic as well (i.e. proton transfer after intersystem crossing). However, since the accessible triplet states are lower in energy than the photoexcited singlet state, part of the excited state drive may already consumed in intersystem crossing, rendering the triplet states less photobasic. The lesson, therefore, is to interpret figure 7 as a thermodynamic guide that depicts necessary conditions for proton transfer, but on its own is not sufficient to predict its kinetic feasibility. Computing the kinetics of proton transfer is more complicated and beyond the scope of this work.

4 Conclusions

We have highlighted the challenges towards chemical application of photobases, with particular emphasis and experimental results on donor-acceptor pre-association, excited state solvation threshold, and engineering the optical gap of photobases while retaining their properties. Our results show that driving bimolecular reactions such as proton capture from a molecule by the photobase requires overcoming the entropic cost of ground state pre-association. In the case studied here it was only possible by increasing the concentration of the donor relative to acceptor by a factor of more than 100. An interesting result of this work is that not all ground state pre-associated molecules undergo proton transfer, even in the presence of a large pK_a difference. It is necessary to have a desirable solvation environment to stabilize the photoproducts (conjugate acid and base). We have found that to achieve such an environment, the donor concentration needed to be increased even further to allow solvation of deprotonated donor amongst a cluster of molecules of its own kind. Covalently tethering photobases near catalytic sites, as has been explored by us previously[36], and exploring solvents that would facilitate hydrogen bonding in the ground state and charge separation in the excited state are possible directions of further investigations.

We have also found some design trends for tuning the optical gap for photobases, with the intention of finding molecules that will achieve photobasicity at lower excitation energies. We have realized that this design space, at least in the dimensions studied here, is rather constrained. Increasing the conjugation size lowers the optical gap, but also adversely affect photobasicity. Tuning the gap via substituents is more efficient for smaller conjugated systems. Our study lays the foundation for exploring this design space further. For example, multiple substituents, multiple heterocyclic nitrogens or other heteroatoms in the conjugated system, exploring non-benzene rings, and identifying the influence of triplet states on the photobase kinetics are all potentially fruitful directions of future work.

5 Experimental and Computational Methods

We took the absorption and emission spectra for a series of eleven solutions, each with varying mole concentration ratios of 5-methoxyquinoline (MeOQ) to trifluoroethanol (TFE) in dichloromethane (DCM). These ratios were 10^2,2×10^2,5×10^2,10^3,2×10^3,5×10^3,10^4,2×10^4,5×10^4,10^5, and 2×10^5. We also performed these experiments in bulk DCM and TFE. In all cases, the concentration of MeOQ was $5\times10^{-}5$ M. All chemicals were purchased from Sigma-Aldrich and used without further purification.

Absorption spectra were obtained using a Cary 50 UV/Vis spectrophotometer. Measurements were made in a 1cm fused quartz cuvette. Absorption spectra were background subtracted and normalized for analysis. In order to analyze the absorption data, we fit the spectra at the concentration ratio extremes (10^2 and 5×10^4) to three Gaussians using MATLAB[47]. We did so to obtain robust analytical forms of these spectra, not to extract physical significance. The absorption spectra at each TFE concentration ratio was then fit as a linear combination of these two basis spectra. The contribution of the hydrogen-bonded basis spectrum was used as a measure of the relative hydrogen-bonded MeOQ population. These values are shown in the blue curve in figure 3. We chose the spectrum with the donor to acceptor ratio of 10^2 to represent the initial non-hydrogen bonded species, and we chose the spectrum with the donor to acceptor ratio of $5x10^4$ to represent the final state where the photobase was completely hydrogen bonded. We chose to fit the concentration ratio of $5x10^4$, rather than the higher ratios of 10^5 or $2x10^5$, in order to ignore any bulk dielectric effects accompanying the introduction of TFE as a significant volumetric component of the solvent. At these higher ratios a blue shift in the absorption spectrum of almost 1 nm was observed, contrary to the red shifting pattern seen at lower concentrations. The red shift indicative of an increase in hydrogen bonded population had completed by a ratio of $5x10^4$, so we are confident that this choice in basis spectrum is appropriate.

Emission spectra were collected on a Jobin-Yvon Fluoromax 3 fluorometer. Measurements were made in a 1 cm fused quartz cuvette. All samples were excited at 310 nm. For the emission data, there was no straightforward choice of basis spectra due to the convolution of ground-state hydrogen bonding effects and excited state proton transfer. Instead, we chose to plot the emission intensities at 575 nm as a function of TFE concentration, normalized with respect to minimum and maximum intensities. These values are shown in the red curve in figure 3. Because there is virtually no emission intensity from the unprotonated form at 575 nm, we can be confident that the rise in intensity we see is due entirely to the rise of the protonated form of MeOQ. After the onset of emission from the protonated form of MeOQ, a clear trend with respect to growth of emission from the protonated form was observed and most of the emission spectra shared an isosbestic point at approximately 450 nm. Two of the collected spectra were offset in the overall emission intensity, but not in the relative peak ratios, likely due to scattering at the sample. To correct for this deviation, we multiplied each spectrum by a constant in order to enforce the isosbestic point at 450 nm.

Electronic structure calculations of quinolines, acridines, and benzacridines were carried out using the Q-Chem software[48]. Ground state geometries were optimized using the ωB97x-D/6-31+G* level of theory. Singlet excited states were then calculated with the TDDFT/ωB97x-D/6-31+G* level of theory. Lowdin charge densities were used for population analysis. The excited states chosen for analysis in all cases were the singlet L_b states, identified via transition dipole moment. Electron density difference maps in figure 5 were visualized with VMD[49].

Details of the determination of experimental ΔpK_a of the 5-substituted quinolines seen in Figure 6 can be found in a previous publication[26].

Conflicts of interest

The authors declare no conflict of interest.

Acknowledgements

The authors gratefully acknowledge support from the NSF CAREER Award (1454467), the NSF Graduate Research Fellowship,

and the Cottrell Scholar Award from the Research Corporation.

Notes and references

1 T. Förster, *Zeitschrift fÃijr Elektrochemie und angewandte physikalische Chemie*, 1950, **54**, 42–46.

2 A. Weller, *Prog. React. Kinet. Mec.*, 1961, **1**, 187–214.

3 L. M. Tolbert and K. M. Solntsev, *Acc. Chem. Res.*, 2002, **35**, 19–27.

4 R. Simkovitch, K. Akulov, S. Shomer, M. E. Roth, D. Shabat, T. Schwartz and D. Huppert, *J. Phys. Chem. A*, 2014, **118**, 4425–43.

5 R. Simkovitch, S. Shomer, R. Gepshtein and D. Huppert, *J. Phys. Chem. B*, 2015, **119**, 2253–2262.

6 D. Pines, E. T. J. Nibbering and E. Pines, *Isr. J. Chem.*, 2015, **55**, 1240–1251.

7 E. Pines and D. Huppert, *J. Phys. Chem.*, 1983, **87**, 4471–4478.

8 D. Spry, A. Goun and M. Fayer, *J. Phys. Chem. A*, 2007, **111**, 230–237.

9 D. B. Spry and M. D. Fayer, *J. Chem. Phys.*, 2008, **128**, 084508.

10 M. Gutman, D. Huppert and E. Pines, *J. Am. Chem. Soc.*, 1981, **103**, 3709–3713.

11 N. Agmon, *J. Phys. Chem. A*, 2005, **1019**, 13–35.

12 M. Prémont-Schwarz, T. Barak, D. Pines, E. T. J. Nibbering and E. Pines, *J. Phys. Chem. B*, 2013, **117**, 4594–4603.

13 S. Abbruzzetti, E. Crema, L. Masino, A. Vecli, C. Viappiani, J. R. Small, L. J. Libertini and E. W. Small, *Biophys. J.*, 2000, **78**, 405–415.

14 T. P. Causgrove and R. B. Dyer, *J. Chem. Phys.*, 2006, **323**, 2–10.

15 J. L. Dempsey, J. R. Winkler and H. B. Gray, *J. Am. Chem. Soc.*, 2010, **132**, 16774–16776.

16 S. Kohse, A. Neubauer, A. Pazidis, S. Lochbrunner and U. Kragl, *J. Am. Chem. Soc.*, 2013, **135**, 9407–9411.

17 H. Peretz-Soroka, A. Pevzner, G. Davidi, V. Naddaka, M. Kwiat, D. Huppert and F. Patolsky, *Nano Lett.*, 2015, **15**, 4758–4768.

18 B. K. Keitz and R. H. Grubbs, *J. Am. Chem. Soc.*, 2009, **131**, 2038–2039.

19 A. Das, S. Ayad and K. Hanson, *Org. Lett.*, 2016, **18**, 5416–5419.

20 W. White, C. D. Sanborn, R. S. Reiter, D. M. Fabian and S. Ardo, *J. Am. Chem. Soc.*, 2017, **139**, 11726–11733.

21 S. Haghighat, S. Ostresh and J. M. Dawlaty, *J. Phys. Chem. B*, 2016, **120**, 1002–07.

22 N. Mataga, Y. Kaifu and M. Koizumi, *Bull. Chem. Soc. Jpn.*, 1956, **29**, 373–379.

23 E. Pines, D. Huppert, M. Gutman, N. Nachliel and M. Fishman, *J. Phys. Chem.*, 1986, **90**, 6366–6370.

24 O. Poizat, E. Bardez, G. Buntinx and V. Alain, *J. Phys. Chem. A*, 2004, **108**, 1874–1880.

25 N. Munitz, Y. Avital, D. Pines, E. T. J. Nibbering and E. Pines, *Isr. J. Chem.*, 2009, **49**, 261–272.

26 E. W. Driscoll, J. R. Hunt and J. M. Dawlaty, *J. Phys. Chem. Lett.*, 2016, **7**, 2093–2099.

27 E. W. Driscoll, J. R. Hunt and J. M. Dawlaty, *J. Phys. Chem. A*, 2017, **121**, 7099–7107.

28 W. Sheng, M. Nairat, P. D. Pawlaczyk, E. Mroczka, B. Farris, E. Pines, J. H. Geiger, B. Borhan and M. Dantus, *Angewandte Chemie International Edition*, 2018, 14742–14746.

29 A. Kellmann and Y. Lion, *Photochem. Photobiol.*, 1979, **29**, 217–222.

30 E. Nachliel, Z. Ophir and M. Gutman, *J. Am. Chem. Soc.*, 1987, **109**, 1342–1345.

31 E. T. Ryan, T. Xiang, K. P. Johnston and M. A. Fox, *J. Phys. Chem. A*, 1997, **101**, 1827–1835.

32 T. T. Eisenhart and J. L. Dempsey, *J. Am. Chem. Soc.*, 2014, **136**, 12221–12224.

33 G. Favaro, U. Mazzucato and F. Masetti, *J. Phys. Chem.*, 1973, **77**, 601–604.

34 S. Vogt and S. G. Schulman, *Chem. Phys. Lett.*, 1983, **97**, 450–3.

35 K. Akulov, R. Simkovitch, Y. Erez, R. Gepshtein, T. Schwartz and D. Huppert, *J. Phys. Chem. A*, 2014, **118**, 2470–2479.

36 I. Demianets, J. R. Hunt, J. M. Dawlaty and T. Williams, *Organometallics (under review)*, 2018.

37 J. R. Hunt and J. M. Dawlaty, *The Journal of Physical Chemistry A*, 2018, **122**, 7931–7940.

38 S. Haghighat, S. Ostresh and J. M. Dawlaty, *The Journal of Physical Chemistry B*, 2016, **120**, 1002–1007.

39 T. FÃűrster, *Zeitschrift fÃijr Elektrochemie und angewandte physikalische Chemie*, 1950, **54**, 42–46.

40 J. F. Ireland and P. A. H. Wyatt, *Advances in Physical Organic Chemistry*, 1976, **12**, 131–221.

41 D. Roccatano, G. Colombo, M. Fioroni and A. E. Mark, *Proceedings of the National Academy of Sciences*, 2002, **99**, 12179–12184.

42 R. Chitra and P. E. Smith, *The Journal of Chemical Physics*, 2001, **114**, 426–435.

43 A. Vogel and B. Furniss, *VogelâĂŹs Textbook of Practical Organic Chemistry Including Quantitative Organic Analysis*, 1978.

44 S.-Y. Park, Y. M. Lee, K. Kwac, Y. Jung and O.-H. Kwon, *Chemistry–A European Journal*, 2016, **22**, 4340–4344.

45 E. W. Driscoll, J. R. Hunt and J. M. Dawlaty, *The Journal of Physical Chemistry Letters*, 2016, **7**, 2093–2099.

46 I. Y. Goryacheva, G. MelâĂŹnikov and S. Shtykov, *Journal of Analytical Chemistry*, 2000, **55**, 874–878.

47 MATLAB, *version 7.10.0 (R2010a)*, The MathWorks Inc, Natick, Massachusetts, 2010.

48 Y. Shao, Z. Gan, E. Epifanovsky, A. T. Gilbert, M. Wormit, J. Kussmann, A. W. Lange, A. Behn, J. Deng, X. Feng, D. Ghosh, M. Goldey, P. R. Horn, L. D. Jacobson, I. Kaliman, R. Z. Khaliullin, T. KuÅŻ, A. Landau, J. Liu, E. I. Proynov, Y. M. Rhee, R. M. Richard, M. A. Rohrdanz, R. P. Steele, E. J. Sundstrom, H. L. W. III, P. M. Zimmerman, D. Zuev, B. Albrecht, E. Alguire, B. Austin, G. J. O. Beran, Y. A. Bernard, E. Berquist, K. Brandhorst, K. B. Bravaya, S. T. Brown, D. Casanova, C.-M. Chang, Y. Chen, S. H. Chien, K. D.

Closser, D. L. Crittenden, M. Diedenhofen, R. A. D. Jr., H. Do, A. D. Dutoi, R. G. Edgar, S. Fatehi, L. Fusti-Molnar, A. Ghysels, A. Golubeva-Zadorozhnaya, J. Gomes, M. W. Hanson-Heine, P. H. Harbach, A. W. Hauser, E. G. Hohenstein, Z. C. Holden, T.-C. Jagau, H. Ji, B. Kaduk, K. Khistyaev, J. Kim, J. Kim, R. A. King, P. Klunzinger, D. Kosenkov, T. Kowalczyk, C. M. Krauter, K. U. Lao, A. D. Laurent, K. V. Lawler, S. V. Levchenko, C. Y. Lin, F. Liu, E. Livshits, R. C. Lochan, A. Luenser, P. Manohar, S. F. Manzer, S.-P. Mao, N. Mardirossian, A. V. Marenich, S. A. Maurer, N. J. Mayhall, E. Neuscamman, C. M. Oana, R. Olivares-Amaya, D. P. OâĂŹNeill, J. A. Parkhill, T. M. Perrine, R. Peverati, A. Prociuk, D. R. Rehn, E. Rosta, N. J. Russ, S. M. Sharada, S. Sharma, D. W. Small, A. Sodt, T. Stein, D. StÃijck, Y.-C. Su, A. J. Thom, T. Tsuchimochi, V. Vanovschi, L. Vogt, O. Vydrov, T. Wang, M. A. Watson, J. Wenzel, A. White, C. F. Williams, J. Yang, S. Yeganeh, S. R. Yost, Z.-Q. You, I. Y. Zhang, X. Zhang, Y. Zhao, B. R. Brooks, G. K. Chan, D. M. Chipman, C. J. Cramer, W. A. G. III, M. S. Gordon, W. J. Hehre, A. Klamt, H. F. S. III, M. W. Schmidt, C. D. Sherrill, D. G. Truhlar, A. Warshel, X. Xu, A. Aspuru-Guzik, R. Baer, A. T. Bell, N. A. Besley, J.-D. Chai, A. Dreuw, B. D. Dunietz, T. R. Furlani, S. R. Gwaltney, C.-P. Hsu, Y. Jung, J. Kong, D. S. Lambrecht, W. Liang, C. Ochsenfeld, V. A. Rassolov, L. V. Slipchenko, J. E. Subotnik, T. V. Voorhis, J. M. Herbert, A. I. Krylov, P. M. Gill and M. Head-Gordon, *Molecular Physics*, 2015, **113**, 184–215.

49 W. Humphrey, A. Dalke and K. Schulten, *Journal of Molecular Graphics*, 1996, **14**, 33–38.